



Electrocatalytic reduction of dioxygen at a modified glassy carbon electrode based on Nafion[®]-dispersed single-walled carbon nanotubes and cobalt–porphyrin with palladium nanoparticles in acidic media

Mohammad Shamsuddin Ahmed, Haesang Jeong, Jung-Min You, Seungwon Jeon*

Department of Chemistry and Institute of Basic Science, Chonnam National University, Gwangju 500-757, Republic of Korea

ARTICLE INFO

Article history:

Received 2 December 2010
Received in revised form 16 February 2011
Accepted 20 February 2011
Available online 1 March 2011

Keywords:

Dioxygen reduction
Electrocatalytic
Cobalt (II) porphyrin
Hydrodynamic voltammetry
Palladium nanoparticles

ABSTRACT

Cathodic dioxygen (O₂) reduction was performed at a modified glassy carbon electrode (GCE) by single-walled carbon nanotubes (SWCNT)/Nafion[®] (NF) film with cobalt (II) tetra (2-amino-phenyl) porphyrin (CoTAPP) and palladium (Pd) nanoparticles incorporated and employed as doping agents. Both the electrochemical behavior of SWCNT with a P(CoTAPP)–Pd nanoparticle matrix and the electrocatalytic reduction of O₂ were investigated using transmission electron microscopy (TEM), cyclic voltammetry (CV) and rotating ring-disk electrode (RRDE) techniques in 0.1 mol l⁻¹ H₂SO₄ aqueous solutions. The electrocatalytic reduction of O₂ at the SWCNT/NF/P(CoTAPP)–Pd composite film established a pathway of four-electron transfer reductions into H₂O. Hydrodynamic voltammetry revealed that the modified electrode was catalyzed effectively by the four-electron transferred reduction of dioxygen into H₂O with minimal generation of H₂O₂. The SWCNT/NF/P(CoTAPP)–Pd composite film showed a highly efficient electrocatalytic performance. P(CoTAPP)–Pd was an effective mediator for the reduction of dioxygen and was responsible for the enhanced catalytic activity.

© 2011 Elsevier Ltd. All rights reserved.

1. Introduction

Over the last few decades, significant effort has been directed towards the development of low-cost electrocatalysts for oxygen reduction reactions (ORR). Finding a low-cost electrocatalyst for ORR is important for practical applications in clean energy generation systems such as fuel cells and metal-air batteries [1,2]. The determination of O₂ is also an important analytical target in biological areas [3]. Oxygen can be measured using electrochemical methods in order to gain the advantages of high sensitivity and selectivity. Several studies have examined the electrocatalytic reduction of O₂ at metalloporphyrin-modified electrodes [4–10]. Cobalt [11–13], copper [14] and iron [14,15] porphyrins have been used as homogeneous catalysts. In the presence of an effective catalyst in aqueous solution, dioxygen can be reduced to H₂O₂ or water via two or four-electron transfer. Some complexes applied as homogeneous catalysts react slowly with O₂; most of them are insoluble in aqueous media. Surface modification of electrodes with carbon nanotubes (CNTs) has led to recent developments in the field of electrocatalysis. Among such developments, detection of bio-organic and inorganic compounds at the CNT matrices has been widely reported [16–19]. CNTs exhibit a π -conjugative

structure with a highly hydrophobic surface [20], a property that allows CNT interaction with various compounds through π – π electronic and hydrophobic interactions [21–23]. CNTs are also used for the preparation of sandwiched film-modified electrodes for electrocatalytic study [24,25]. Similarly, electropolymerization is a simple but powerful method used to target selective modification of different types of electrodes with desired matrices. Numerous conjugated polymers (porphyrin) have been electrochemically synthesized for fabrication of chemical and biochemical sensor devices [4–10]. The conjugated polymers used for sensor devices exhibit interesting enhancements in the electrocatalytic activity towards oxidation or reduction [20]. Oxygen is reduced through a complicated series of reactions involving the formation of a H₂O₂ intermediate [26]. Analysis of H₂O₂ formation can provide additional information regarding the effects on the reaction mechanism. RRDE is used to determine kinetic parameters for O₂ reduction and to detect intermediate formation. It is generally recognized that NF has a microscopically phase-separated structure that consists of hydrophilic ionic clusters, a hydrophobic backbone and an intermediate region [27–30]. Impregnation of NF into gas-diffusion electrodes in proton exchange membrane fuel cells (PEMFCs) should affect the mass-transport, and the electrode kinetics of the fuel cell reactions [31]. Many research groups have reported that the presence of an NF film does enhance the kinetic current for O₂ reduction at NF-coated Pt electrodes [32–34]. To develop a low cost ORR electrocatalyst, Pd nanoparticles were

* Corresponding author. Tel.: +82 62 530 0064; fax: +82 62 530 3389.
E-mail address: swjeon3380@naver.com (S. Jeon).

preferred over platinum and gold due to the lower price. Palladium has been reported to present considerable catalytic activity for ORR in acidic electrolyte solution and preferentially proceeds through a four-electron pathway, which is important for oxygen sensing [35]. Few research groups have used only Pd nanoparticles in ORR.

In the present work, we have explored the P(CoTAPP)–Pd architectures whereby the molecules oriented on the surface of the electrodes by electrochemistry were used in the electroreduction of O₂. The SWCNT/NF-coated GCE was covered with P(CoTAPP)–Pd using electropolymerization in a 0.1 mol l⁻¹ tetrabutylammonium perchlorate (TBAP)/acetonitrile (AN) solution and further chemically processed. In order to provide a stronger understanding of the potential and currents of SWCNT/NF/P(CoTAPP)–Pd composite film in the reduction of dioxygen in 0.1 mol l⁻¹ H₂SO₄ aqueous solutions, the electrochemical behavior, stability and electrocatalytic activity towards ORR of the newly synthesized composite electrode were electrochemically analyzed using CV and RRDE techniques.

2. Experimental

2.1. Instruments

Voltammetric measurements were accomplished with a three-electrode potentiostat [CHI 700C electrochemical workstation (USA)] in a grounded Faraday cage. A platinum-wire electrode separated from the analyte compartment by a medium porosity glass frit was used as an auxiliary electrode. A calibrated Ag/AgCl electrode [3 M NaCl solution] supplied by Bioanalytical Systems Inc. (BAS) was used as a reference electrode, with a potential of approximately 45 mV relative to a saturated calomel electrode (SCE). A GCE (3 mm in diameter) was employed as a working electrode after modification with a composite film. An EG&PARC Model 636 RRDE system and a CHI 700C electrochemical workstation bipotentiostat were used for hydrodynamic voltammetry experiments. A rotating GC disk (4.3 mm in diameter)–platinum ring electrode was used as a working electrode. Electrochemical impedance spectroscopy (EIS) was performed with a Versa State 3, manufactured by Metek, USA. Transmission electron microscopy (TEM) images were taken by a TECNAI model FI-20 (FEI, Netherland) in ethanol after 20 min ultrasonication. The dioxygen concentration in the dioxygen-saturated solution was 1.2 mM (similar to Ref. [13]). All potentials were recorded with respect to the Ag/AgCl electrode at room temperature (RT).

2.2. Chemicals

CoTAPP was synthesized as described in the literature [36]. The SWCNT (1.2–1.5 nm in diameter produced by the arc method) was purchased from Aldrich (Korea) and purified with 6 M HCl solution. NF (5 wt% in lower aliphatic alcohols and water), PdCl₂ and NaBH₄ were also purchased from Aldrich. All other reagents used were of analytical grade. High purity argon was used for deaeration. All experiments were carried out at RT. Doubly distilled water with resistibility over 18 MΩ cm in a quartz apparatus was used to prepare all aqueous electrolyte solutions. The 0.1 M H₂SO₄ (Fischer Scientific) solution was used as the supporting electrolyte.

2.3. Preparation of working electrodes

An RRDE containing a GC disk and Pt ring sealed in a polytetrafluoroethylene holder was polished with 0.05 μm alumina suspension on a polishing cloth (BAS, USA) and cleaned with ultrasonication in distilled water. After the surface was polished to a mirrored surface, it was electropolished in 10% HCl solution at 1 mA cm⁻² for 30 min to remove any Pt contamination. The solution was replaced with 0.1 mol l⁻¹ H₂SO₄ and hydrogen was evolved at both ring and disk

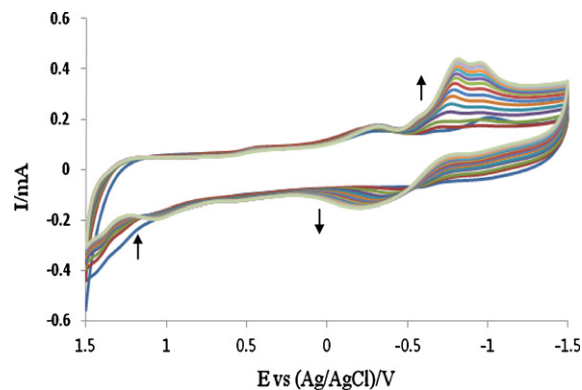


Fig. 1. Electropolymerization of CoTAPP in 0.1 mol l⁻¹ TBAP/AN solution at a scan rate of 100 mV/s.

electrodes for 1 min to desorb chloride ions [31]. The ring collection efficiency ($N=0.18$) was determined using a solution of ferrocene.

Following cleaning, the dispersed solution was prepared by dispersion of 1.0 mg SWCNT and 0.5 ml NF in 0.5 ml AN to generate a black solution. For a homogeneous suspension, the solution was sonicated with ultrasonic agitation for 30 min. To prepare the SWCNT/NF/GCE-modified electrode, 4 × 2 μl of the black solution was cast onto the GCE surface and the solvent evaporated at RT. After coating, electropolymerization of CoTAPP (2.0 mg CoTAPP in 4.0 ml 0.1 M TBAP/AN solution) was performed between sweeping potentials +1.5 V to –1.5 V at 0.1 V/s for 15 cycles (Fig. 1). The partially modified electrode was soaked in 0.25 wt% PdCl₂ and 0.5 wt% NaBH₄ aqueous solution for 20 min and 60 min, respectively, to prepare the Pd nanoparticles (Pd⁰). Finally, electrode was washed several times with distilled water. Electrochemical measurements using the SWCNT/NF/P(CoTAPP)–Pd modified electrode were conducted in Ar and dioxygen-saturated 0.1 M H₂SO₄ solution for the electrocatalytic reduction of O₂.

3. Results and discussion

3.1. TEM studies of SWCNT/NF/P(CoTAPP)–Pd film

TEM is a powerful instrument that was used to observe the surface of the nanoparticles. The morphology of the SWCNT/NF/P(CoTAPP)–Pd composite film was investigated by TEM. Fig. 2 displays the TEM micrographs of the composite film. Fig. 2a demonstrates that Pd nanoparticles were set successfully onto an electropolymerized SWCNT/NF film; large Pd nanoparticles were found on the surface of SWCNT/NF/P(CoTAPP). Approximately 5–10 nm nanoparticles were cast on the modified electrode (Fig. 2b).

3.2. EIS measurement

EIS is an important experiment that provides information about impedance of the electrode. It is well known that the Nyquist plot has two regions: the first is a semicircular portion and the second is the linear portion. The semicircular portion at higher frequencies corresponds to the electron-transfer limited process which controls the electron transfer kinetics of the redox probe at the electrode interface. The linear portion at lower frequencies corresponds to the diffusion process. As shown in Fig. 3, the Nyquist plots display the impedance spectroscopy of (i) bare GCE, (ii) SWCNT/NF/P(CoTAPP)–Pd/GCE and (iii) SWCNT/NF/P(CoTAPP)/GCE in 0.1 mol l⁻¹ KCl containing 5.0 mM K₃Fe(CN)₆/K₄Fe(CN)₆ (1:1) by applied frequency from 10⁵ Hz to 10⁻² Hz. The bare GCE showed a large semicircle up to 2.8 kΩ, indicating that the bare GCE was

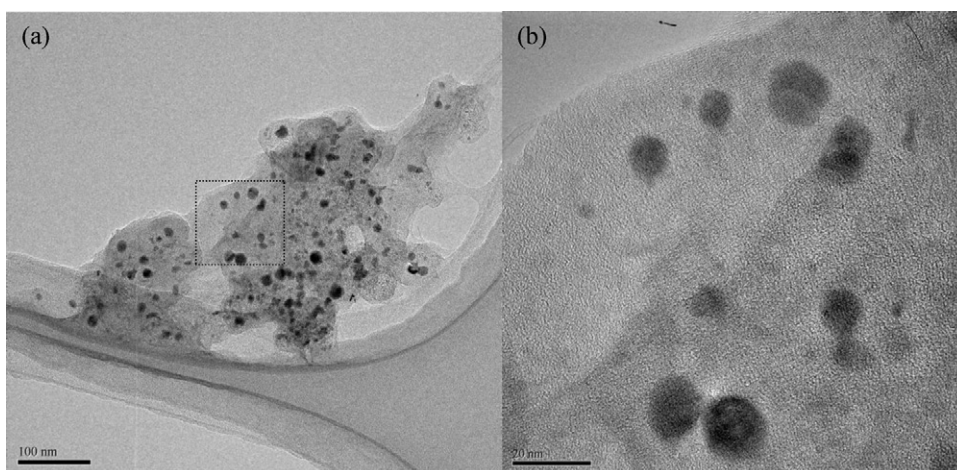


Fig. 2. TEM images of SWCNT/NF/P(CoTAPP)-Pd.

an obstacle and made the electron transfer at the interface more difficult when compared to other modified GCEs. A very small semi-circle portion for both (ii) SWCNT/NF/P(CoTAPP)-Pd/GCE and (iii) SWCNT/NF/P(CoTAPP)/GCE, and they showed small resistances of 150 Ω and 223 Ω , respectively. The results indicated that both modified GCE electrodes were highly conductive and made the electron transfer at the interface easier than with a bare GCE.

3.3. Electrocatalytic O_2 reduction on SWCNT/NF/P(CoTAPP)-Pd/GCE

The SWCNT/NF/P(CoTAPP)-Pd/GCE electrode was employed for the reduction of molecular oxygen in this study via CV. The peak potential of the dioxygen reduction wave appeared for the SWCNT/NF/P(CoTAPP)-Pd-coated electrodes. Typical CVs were taken in Ar and oxygen saturated 0.1 mol l⁻¹ H₂SO₄ solutions, and all had potentials ranging from 0.6 V to -0.1 V at scan rate of 25 mV/s, shown in Fig. 4. As expected, there was a negligible peak potential for Ar saturated CV. A significant and clear peak potential appeared at 0.21 V for the O₂ saturated acid solution and had a current response of 41 μ A (much higher than Refs. [11,13]). The reduction reaction started from 0.5 V, while the peak currents increased linearly (correlation coefficient 0.997) with the square root of the scan rates (Fig. 4 inset). The study suggested that the electrocatalytic processes were controlled by molecular oxygen diffusion in a modified electrode [37]. In a typical irreversible reaction, the relationship between the peak current and scan rate was as

follows [13,38]:

$$i_p = 0.4958nFA \left(\frac{\alpha n_\alpha F}{RT} \right)^{1/2} \nu^{1/2} D^{1/2} \quad (1)$$

$$\Delta E_p = \frac{1.15RT}{\alpha n_\alpha F} \quad (2)$$

where n is the number of transferred electrons, A is the surface area of the GCE (surface area of 0.070686 cm² was employed) and D and C are the oxygen diffusion coefficient and the bulk concentration, respectively. The value of the oxygen diffusion coefficient was 1.9E-5 cm²/s, ν is the scan rate in V/s, α is the transfer coefficient, n_α is the apparent number of electrons transferred in the rate-determining step and ΔE_p is the peak potential change when the scan rate increases 10-fold. Other symbols mentioned used their standard values. The number of transferred electrons was calculated as 3.4 for the reduction of O₂ using Eq. (1). No anodic peak was present, indicating that the catalytic reduction reaction process was irreversible in the experiment.

3.4. Hydrodynamic voltammetry

To analyze experimental results in this study, we used a simplified model [39] shown in Scheme 1. Path 1 shows how O₂ is reduced directly to H₂O through a four-electron transfer. Path 2 is the sequential reaction path where O₂ is first reduced to H₂O₂ through a two-electron transfer followed by a two-electron reduction to H₂O (Path 3), or by the release of the formed H₂O₂ into bulk solution (Path 4).

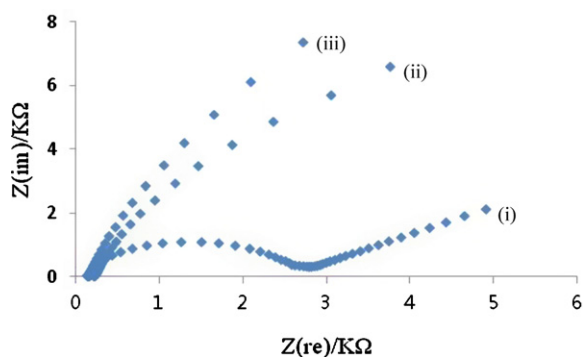


Fig. 3. Nyquist plots of (i) bare GCE, (ii) SWCNT/NF/P(CoTAPP)-Pd and (iii) SWCNT/NF/P(CoTAPP).

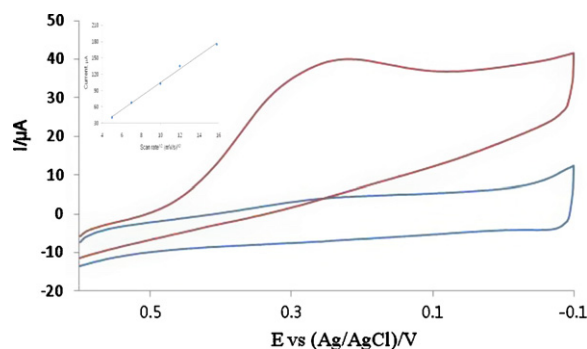
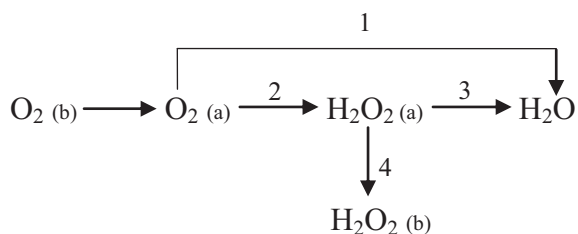


Fig. 4. CVs of SWCNT/NF/P(CoTAPP)-Pd electrode in Ar- and O₂-saturated 0.1 mol l⁻¹ H₂SO₄ solution at 25 mV/s; inset: plot of peak current versus square root of scan rate.



Scheme 1. A model for ORR (a) adsorbed on electrode surface and (b) in bulk solution.

The RRDE experiments of hydrodynamic voltammetry were useful in confirming the electrocatalytic reduction pathway of O_2 . The electrocatalytic O_2 reduction activity determined by the RRDE method using SWCNT/NF/P(CoTAPP) and SWCNT/NF/P(CoTAPP)-Pd-modified electrodes were investigated in $0.1 \text{ mol l}^{-1} \text{ H}_2\text{SO}_4$ solution under O_2 saturated conditions at a rotation speed of 25–2500 rpm. The disk potential employed was from +0.5 V to –0.5 V at 20 mV/s, and the ring potential was constant at 1.2 V (Fig. 5). In Fig. 5, the RRDE voltammograms were obtained from the SWCNT/NF/P(CoTAPP)-modified electrodes; the O_2 reduction started at approximately 0.3 V and the current response was significantly high. The Koutecky–Levich equation [40] was used for the calculation of the n value as follows:

$$i_{\text{lim}} = 0.62nFAD^{2/3}C\omega^{1/2}\nu^{-1/6} \quad (3)$$

where i_{lim} is the limiting current (μA) on the plateau, ω is angular velocity (rad/s), ν is the kinematic viscosity (cm^2/s), the kinematic viscosity was $0.01 \text{ cm}^2/\text{s}$ and n is the electron number. The Koutecky–Levich plots for the RRDE voltammograms of SWCNT/NF/P(CoTAPP) obtained at various rpm are shown in Fig. 6. The solid lines were obtained from the plateau current. The dependence of transferred electrons on the cathodic potential was calculated from Eq. (3). According to the n value of the reaction, two electrons were involved, which indicated that the primary product was H_2O_2 . Nevertheless, the RRDE voltammograms (in +0.6 V to –0.2 V at 20 mV/s, ring potential of 1.2 V) exhibited by the SWCNT/NF/P(CoTAPP)-Pd-modified electrode (Fig. 7) showed that O_2 reduction started from a more positive potential (approximately 0.5 V) and the current response was higher than without Pd nanoparticle modified electrodes (comparable to Ref. [11]). The

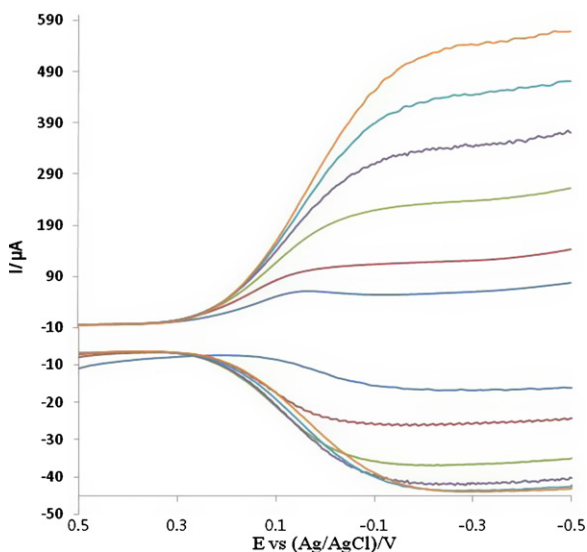


Fig. 5. RRDE voltammograms obtained from SWCNT/NF/P(CoTAPP) at 25, 100, 400, 900, 1600 and 2500 rpm; ring potential was constant at 1.2 V; scan rate of 20 mV/s.

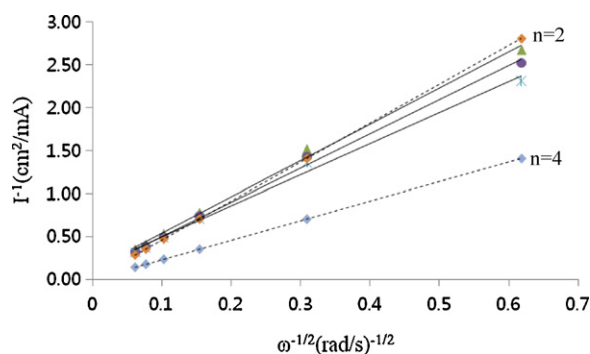


Fig. 6. Koutecky–Levich plots for ORR catalyzed by SWCNT/NF/P(CoTAPP) at –0.1, –0.2 and –0.3 V applied potentials.

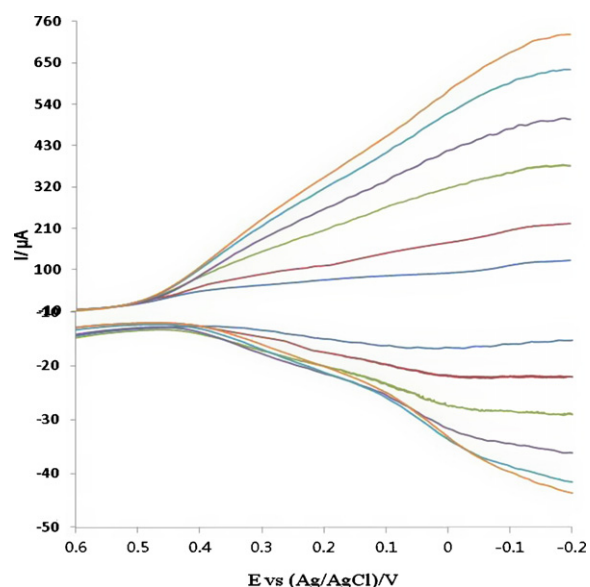


Fig. 7. RRDE voltammograms recorded from SWCNT/NF/P(CoTAPP)-Pd at 25, 100, 400, 900, 1600 and 2500 rpm; ring potential remained constant at 1.2 V; scan rate of 20 mV/s.

initial potentials were used in order to determine the potential at which the electrocatalytic activity began, which defined the potentials and the O_2 reduction wave departures from the baseline in both cases. The Koutecky–Levich plots are shown in Fig. 8 (data obtained from Fig. 7). The n values were also calculated by Eq. (3). The two dashed lines were calculated theoretically for two and four electrons in both Figs. 6 and 8. According to the n value, four electrons were involved, which indicated the main product to be H_2O .

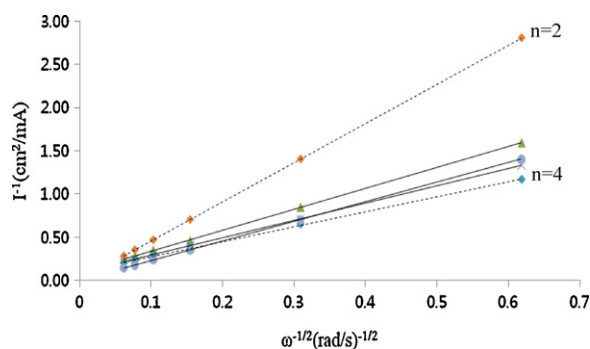


Fig. 8. Koutecky–Levich plots for ORR catalyzed by SWCNT/NF/P(CoTAPP)-Pd at 0.0, –0.1 and –0.2 V applied potentials.

Table 1
Comparison of two modified GCE electrodes.

SWCNT/NF/P(CoTAPP)				SWCNT/NF/P(CoTAPP)–Pd			
E/V	n value	Koutecky–Levich plot		E/V	n value	Koutecky–Levich plot	
		Slope	R ²			Slope	R ²
–0.1	2.1	4.220	0.996	0.0	3.6	2.418	0.999
–0.2	2.2	3.976	0.996	–0.1	4.2	2.007	0.999
–0.3	2.4	3.617	0.993	–0.2	4.4	1.728	0.999

The Koutecky–Levich plots were straight lines with distinct slope and intercept values that were not equal to 0. The results indicated that the ORR was not controlled solely by diffusion limited processes [41].

As seen in Table 1, the slope is inversely proportional to the number of electrons transferred per oxygen molecule [42]. Hydrogen peroxide and water were produced when O₂ was reduced by two and four electrons. The percentage (%) of H₂O₂ was calculated with the following equation [42]:

$$\%H_2O_2 = \frac{i_r/i_d}{N} \times 100 \quad (4)$$

where i_r and i_d are the ring and disk limiting current, respectively. Ring currents corresponding with the formation of H₂O₂ were observed under such conditions. For example, the H₂O₂ percentage was 78% and 41% at 400 rpm when catalyzed by SWCNT/NF/P(CoTAPP) and SWCNT/NF/P(CoTAPP)–Pd electrodes, respectively. The intermediate H₂O₂ production was decreased with increasing rpm and vice versa.

3.5. Tafel behavior

To further analyze the kinetics of the dioxygen reduction reaction, Tafel behavior in the mixed kinetic-diffusion control region was also examined using the conventional method of constructing Tafel plots for SWCNT/NF/P(CoTAPP) (Fig. 9a) and SWCNT/NF/P(CoTAPP)–Pd-modified GCE (Fig. 9b). The approxi-

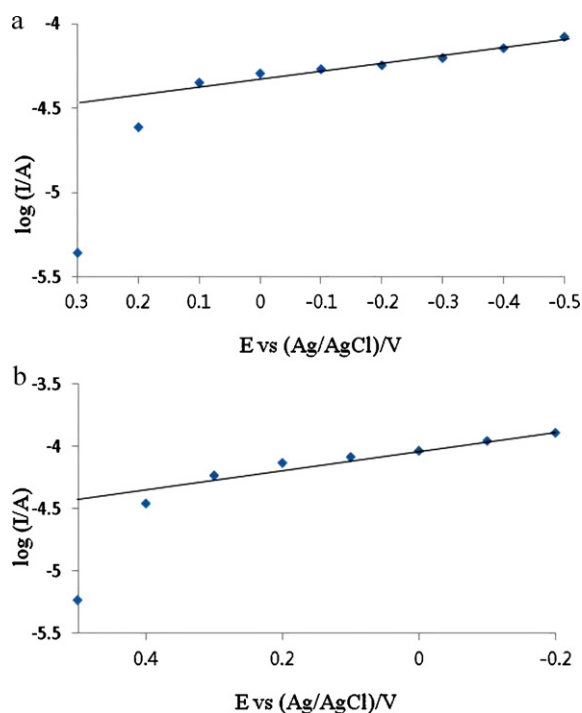


Fig. 9. Tafel Plots for (a) SWCNT/NF/P(CoTAPP) and (b) SWCNT/NF/P(CoTAPP)–Pd at 25 rpm at the sited potential range.

mate straight-line portion was observed in the region and every Tafel curve exhibited two distinct regions of different slopes, generally seen in Tafel plots [41]. However, both plots were linear at disk potentials 0.1 to –0.5 for plot (a) and 0.3 to –0.2 for plot (b). The Tafel slopes at 25 rpm were –0.421 and –0.659 V/decade for SWCNT/NF/P(CoTAPP) and SWCNT/NF/P(CoTAPP)–Pd, respectively. The data indicated that the rate-determining step for O₂ reduction was identical at both modified electrodes. Each plot in Fig. 9 turns aside into the band and the kinetic current decreased with a drop in potential. This result was likely due to surface blocking by intermediate H₂O₂ [31]. However, the Tafel slopes were not close to each other, indicating that there was a significant effect from the Pd nanoparticle coating on the kinetics and reaction mechanism. This phenomenon could be due to the variation in transferred electron number. The numbers of transferred electrons were calculated as 2.2 and 3.5 by the above Tafel slopes [38] for SWCNT/NF/P(CoTAPP) and SWCNT/NF/P(CoTAPP)–Pd, respectively.

4. Conclusions

The kinetics of cathodic O₂ reduction were examined at a SWCNT/NF/P(CoTAPP)–Pd-modified GCE. A combination of CV, RRDE and TEM techniques was used to investigate the behavior of SWCNT/NF/P(CoTAPP)–Pd-modified GCE for ORR in 0.1 mol l^{–1} H₂SO₄ aqueous solutions. The study covered a potential range between 0.6 V and –0.1 V (for CV) and 0.6 V to –0.5 V (for hydrodynamic voltammetry), with attention given to the ORR process. A fully developed reduction peak at 0.2 V (CV) was observed, which represented the reduction of O₂. The peak currents were proportional to the square root of the scan rate. No oxidation peak was present, indicating that the reaction was irreversible. RRDE was employed to determine the kinetic parameters for O₂ reduction and to detect intermediate H₂O₂ formation. The ORR started from at a higher positive potential (0.5 V). The Koutecky–Levich equation and plots were used for the determination of transferred electrons and to verify that the ORR was not diffusion controlled. The CV and RRDE results confirmed that water was the major product of O₂ reduction by the SWCNT/NF/P(CoTAPP)–Pd-modified GCE via four-electron transfer.

Acknowledgement

This research was supported by the science research program through the National Research Foundation of Korea (NRF) funded by the Ministry of Education, Science and Technology (2010-0007864).

References

- [1] C.W.B. Bezerra, L. Zhang, K. Lee, H. Liu, A.L.B. Marques, E.P. Marques, H. Wang, J. Zhang, *Electrochim. Acta* 53 (2008) 4937–4951.
- [2] E.T. Wood, Z.S. Tan, K.A. Schmoedel, D. O'Neill, R. Atanasoski, *J. Power Sources* 178 (2008) 510–516.
- [3] Y. Komai, *J. Exp. Biol.* 201 (1998) 2359.
- [4] J. Qu, Y. Shen, X. Qu, S. Dong, *Electroanalysis* 16 (2004) 1444.

- [5] S. Fukuzumi, K. Okamoto, C.P. Gros, R. Guillard, *J. Am. Chem. Soc.* 126 (2004) 10441.
- [6] H. Winnischofer, V.Y. Otake, S. Dovidauskas, M. Nakamura, H.E. Toma, K. Araki, *Electrochim. Acta* 49 (2004) 3711.
- [7] E.S. Ribeiro, Y. Gushikem, J.C. Biazotto, O.A. Serra, *J. Porphyr. Phthalocyan.* 6 (2002) 527.
- [8] A.L. Bouwkamp-Wijnoltz, W. Visscher, J.A.R. van Veen, E. Boellaard, A.M. van der Kraan, S.C. Tang, *J. Phys. Chem. B* 106 (2002) 12993.
- [9] B. Shentu, K. Oyaizu, H. Nishide, *Chem. Lett.* 7 (2002) 712.
- [10] C.A. Pessoa, Y. Gushikem, *J. Porphyr. Phthalocyan.* 5 (2001) 537.
- [11] A. Choi, H. Jeong, S. Kim, S. Jo, S. Jeon, *Electrochim. Acta* 53 (2008) 2579–2584.
- [12] H. Liu, L. Zhang, J. Zhang, D. Ghosh, J. Jung, B.W. Downing, E. Whittemore, *J. Power Sources* 161 (2006) 743–752.
- [13] G. Zuo, H. Yuan, J. Yang, R. Zuo, X. Lu, *J. Mol. Catal. A: Chem.* 269 (2007) 46–52.
- [14] T. Yamaguchi, K. Tsukamoto, O. Ikeda, R. Tanaka, T. Kuwabara, K. Takahashi, *Electrochim. Acta* 55 (2010) 6042–6048.
- [15] D. Ricard, A. Didier, M. L'Her, B. Boitrel, *Comptes Rendus Chimie* 5 (2002) 33–36.
- [16] G. Wu, Y.S. Chen, B.Q. Xu, *Electrochem. Commun.* 7 (2005) 1237.
- [17] J.S. Ye, Y. Wen, W.D. Zhang, H.F. Cui, G.Q. Xu, F.S. Sheu, *Nanotechnology* 17 (2006) 3994.
- [18] U. Yogeswaran, S.M. Chen, *Electrochim. Acta* 52 (2007) 5985.
- [19] J. Wang, M. Li, Z. Shi, N. Li, Z. Gu, *Electrochim. Acta* 47 (2001) 651.
- [20] Y. Umasankar, J.-W. Shie, S.-M. Chen, *J. Electrochem. Soc.* 156 (2009) K238–K244.
- [21] Q. Li, J. Zhang, H. Yan, M. He, Z. Liu, *Carbon* 42 (2004) 287.
- [22] J. Zhang, J.K. Lee, Y. Wu, R.W. Murray, *Nano Lett.* 3 (2003) 403.
- [23] A. Star, T.R. Han, J. Christophe, P. Gabriel, K. Bradley, G. Gruner, *Nano Lett.* 3 (2003) 1421.
- [24] M. Zhang, K. Gong, H. Zhang, L. Mao, *Biosens. Bioelectron.* 20 (2005) 1270.
- [25] R.J. Chen, Y. Zhang, D. Wang, H. Dai, *J. Am. Chem. Soc.* 123 (2001) 3838.
- [26] K. Kinoshita, *Electrochemical Oxygen Technology*, Wiley, New York, 1992.
- [27] T.D. Gierke, W.Y. Wu, in: A. Eisenberg, H.L. Yeager (Eds.), *Perfluorinated Ionomer Membranes*, ACS Symposium Series No. 180, American Chemical Society, Washington, DC, 1982, Chap. 13.
- [28] T.D. Gierke, G.E. Mann, F.C. Wilson, *J. Polym. Sci. Polym. Phys. Ed.* 19 (1981) 1687.
- [29] H.L. Yeager, A. Steck, *J. Electrochem. Soc.* 131 (1984) 1880.
- [30] Z. Ogumi, T. Kuroe, Z. Takehara, *J. Electrochem. Soc.* 132 (1985) 2601.
- [31] J. Maruyama, M. Inaba, Z. Ogumi, *J. Electroanal. Chem.* 458 (1998) 175–182.
- [32] D.R. Lawson, L.D. Whiteley, C.R. Martin, M.N. Szentirmay, J.I. Song, *J. Electrochem. Soc.* 135 (1988) 2247.
- [33] S. Gottesfeld, I.D. Raistrick, S. Srinivasan, *J. Electrochem. Soc.* 134 (1987) 1455.
- [34] J.B. Floriano, E.A. Ticianelli, E.R. Gonzalez, *J. Electroanal. Chem.* 367 (1994) 157.
- [35] I.D. Burbe, J.K. Casey, *J. Electrochem. Soc.* 140 (1993) 1284.
- [36] A.D. Adler, F.R. Longo, F. Kampas, J. Kim, *J. Inorg. Nucl. Chem.* 32 (1970) 2443.
- [37] W. Lu, C. Wang, Q. Lv, X. Zhou, *J. Electroanal. Chem.* 558 (2003) 59.
- [38] A.J. Bard, L.R. Faulkner, *Electrochemical Methods—Fundamentals and Applications*, Wiley, New York, 1980.
- [39] A. Damjanovic, M.A. Genshaw, J.O'M. Bockris, *J. Chem. Phys.* 45 (1966) 4057.
- [40] D.T. Sawyer, A. Sobkowiak, J.L. Roberts Jr., *Electrochemistry for Chemists*, 2nd ed., Wiley, John Wiley & Sons, New York, 1995.
- [41] R.H. Castellanos, A.L. Ocampo, J. Moreira-Acosta, P.J. Sebastian, *Int. J. Hydrogen Energy* 26 (2001) 1301–1306.
- [42] K. Lee, L. Zhang, H. Lui, R. Hui, Z. Shi, J. Zhang, *Electrochim. Acta* 54 (2009) 4704–4711.